Redox-controlled exchange bias in a supramolecular chain of Fe_4 single-molecule magnets

Andrea Nava,[a,b] Luca Rigamonti,[a] Ennio Zangrando,[c] Roberta Sessoli,[d] Wolfgang Wernsdorfer,[e] and Andrea Cornia*[a]

Abstract: *Tetrairon(III) single-molecule magnets $[Fe_4(pPy)_2(dpm)_6]$ (**1**) (H_3pPy = 2-(hydroxymethyl)-2-(pyridin-4-yl)propane-1,3-diol, Hdpm = dipivaloylmethane) have been organized into supramolecular chains by reaction with paddlewheel complexes $[Ru^{II,II}_2(OAc)_4(MeOH)_2]$ and $[Ru^{II,III}_2(OAc)_4(THF)_2](BF_4)$. The products $[Fe_4(pPy)_2(dpm)_6][Ru_2(OAc)_4](BF_4)_x$ with x = 0 (**2a**) or x = 1 (**2b**) differ in the electron count on the diruthenium bridges and display hysteresis loops of substantially different shape. While the diruthenium(II,II) paddlewheels in **2a** act as effective s_{eff} = 0 spins, the mixed-valent (II,III) bridges (s_{eff} = 1/2) in **2b** introduce a significant exchange bias, with concomitant enhancement of the remnant magnetization.*

Single-Molecule Magnets (SMMs) provide nanoscale, chemically-tuneable units that display magnetic hysteresis and quantum magnetism at the molecular level.[1] Their magnetic moment is amenable to be probed and controlled by electric currents or electromagnetic radiation; consequently, SMMs have been proposed as components for molecular spintronic devices[2] or as qubits for quantum computation.[3,4] To this aim, molecules need to be stably interfaced with the environment while preserving their properties.[5] Additionally, weak coupling between two or more SMMs can be used to further enhance their functionality. On one side, each SMM can act as a bias on its neighbour(s), generating a better memory effect. On the other side, entanglement between quantum states is an important resource for quantum information processing.[4] Supramolecular C−H···Cl hydrogen-bonded pairs of Mn_4 clusters (S = 9/2) demonstrated such coupling for the first time.[6] Since then, more supramolecular dimers,[7] chains[8] and 3D networks[9] have been described in which SMMs interact weakly through hydrogen bonds or other short contacts. Anyway, such supramolecular organizations are largely serendipitous in nature and are disrupted upon dissolution. Alternative approaches to exchange-biased SMM aggregates were proposed by Clérac, Christou, Hendrickson *et al.* based on coordination bonds;[10–12] general strategies to controlled association of SMMs into coordination networks have been recently reviewed by Clérac *et al.*.[13]

We herein describe the fully-controlled assembly of a tetrairon(III) SMM[14] with an S = 5 ground state, $[Fe_4(pPy)_2(dpm)_6]$ (**1**), into one-dimensional supramolecular structures held together by coordination bonds. In **1**, Hdpm is dipivaloylmethane and H_3pPy is 2-(hydroxymethyl)-2-(pyridin-4-yl)propane-1,3-diol, a tripodal ligand bearing a 4-pyridyl substituent. This SMM acts as a ditopic supramolecular synthon and reacts with paddlewheel dimers $[Ru_2(OAc)_4(MeOH)_2]$[15] and $[Ru_2(OAc)_4(THF)_2](BF_4)$[16] to give supramolecular chains $[Fe_4(pPy)_2(dpm)_6][Ru_2(OAc)_4](BF_4)_x$ with x = 0 (**2a**) or 1 (**2b**), respectively. The mixed-valent diruthenium paddlewheel and some isostructural 3*d* metal dimers were previously used as linkers between Cr_7Ni rings,[17] but not between SMMs. Both bridging diruthenium units are paramagnetic with s = 1 and 3/2, respectively. However, due to their giant hard-axis anisotropy along the chain direction, at low temperature they act as effective spins with s_{eff} = 0 and 1/2, respectively, showing that intrachain magnetic interactions in these systems are amenable to redox control (Figure 1).

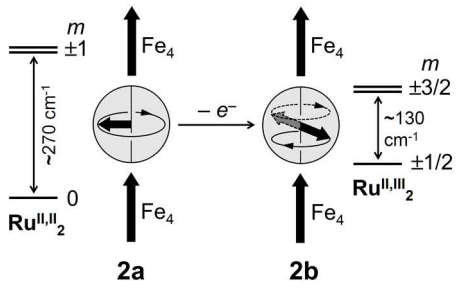

Figure 1. Effect of one-electron oxidation on the magnetic properties of Ru_2 bridges in **2a** and **2b**. Bold arrows depict spin vectors at Fe_4 and Ru_2 sites. The leftmost and rightmost diagrams show the large zero-field splittings that give rise to a nonmagnetic m = 0 ground singlet and an m = ±1/2 ground doublet in $Ru^{II,II}_2$ (s = 1) and $Ru^{II,III}_2$ (s = 3/2), respectively.

Compound **1** was assembled by reaction of the dimer $[Fe_2(OEt)_2(dpm)_4]$ with $FeCl_3$ in the presence of excess tripodal ligand H_3pPy and piperidine as a base in ethanol:diethyl ether. It was isolated as X-ray-quality crystals of **1**·2EtOH by vapour diffusion of ethanol into the reaction mixture. Selected geometrical parameters are reported in Table S1, while the molecular structure is shown in Figure 2.

[a] Mr. A. Nava, Dr. L. Rigamonti, Prof. A. Cornia*
Dipartimento di Scienze Chimiche e Geologiche
Università degli Studi di Modena e Reggio Emilia and INSTM RU of Modena and Reggio Emilia
via G. Campi 183, 41125 Modena, Italy
E-mail: acornia@unimore.it
[b] Mr. A. Nava
Dipartimento di Scienze Fisiche, Informatiche e Matematiche
Università degli Studi di Modena e Reggio Emilia
via G. Campi 183, 41125 Modena, Italy
[c] Prof. E. Zangrando
Dipartimento di Scienze Chimiche e Farmaceutiche
Università degli Studi di Trieste
via L. Giorgieri 1, 34127 Trieste, Italy
[d] Prof. R. Sessoli
Laboratory of Molecular Magnetism (LAMM)
Dipartimento di Chimica 'Ugo Schiff'
Università degli Studi di Firenze & INSTM RU of Florence
Via della Lastruccia 3-13, 50019 Sesto Fiorentino (FI), Italy
[e] Dr. W. Wernsdorfer
Institut Neel, CNRS
25 Rue des Martyrs, BP 166, 38042 Grenoble Cedex 9, France

Supporting information for this article is given via a link at the end of the document.

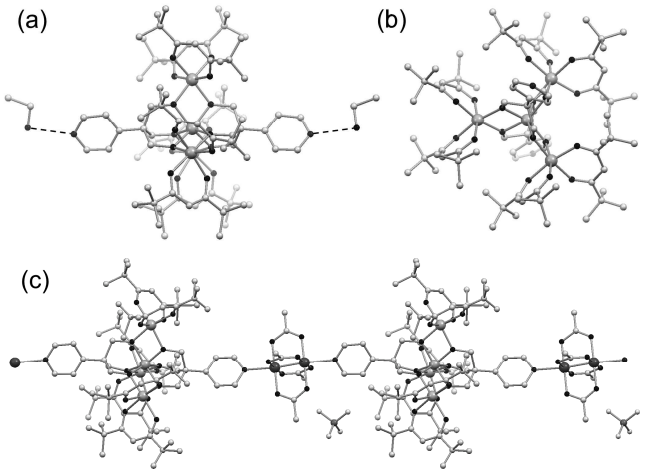

Figure 2. Side view along **c** (a) and top view along **a** (b) of the molecular structure of **1**·2EtOH**.** The side view includes the hydrogen-bonded ethanol molecules in their highest-occupancy position. (c) Structure of **2b** viewed along **b** showing two repeating units running along the **c** axis. Atoms are represented as spheres with: Fe = large light grey, Ru = large dark grey, O/N/B = black, C/F = light grey. Hydrogen atoms are omitted for clarity.

Slow diffusion of a THF solution of the diruthenium(II,II) complex $[Ru_2(OAc)_4(MeOH)_2]$ into a solution of **1**·2EtOH in DCM under inert atmosphere afforded **2a** as tiny red crystals, according to Equation (1) (L = MeOH, x = 0).

$$[Fe_4(pPy)_2(dpm)_6]\cdot 2EtOH + [Ru_2(OAc)_4(L)_2](BF_4)_x \rightarrow [Fe_4(pPy)_2(dpm)_6][Ru_2(OAc)_4](BF_4)_x \ (\mathbf{2a,b}) + 2L + 2EtOH \quad (1)$$

Crystals of **2a** are exceedingly air-sensitive and very weak X-ray diffractors even with synchrotron radiation. A preliminary, low-quality data collection revealed the position of all non-hydrogen atoms and confirmed a polymeric structure with $Fe^c\cdots Ru$ distances of 9.3 Å and markedly nonlinear geometry (in the following, Fe^c and Fe^p will indicate central and peripheral iron ions, respectively). The asymmetric unit contains one tetrairon(III) and one diruthenium(II) complex, with a 43.9° angle between Fe_4 and RuO_4 planes (Figure S1).

Reaction of **1**·2EtOH with the mixed-valent complex $[Ru_2(OAc)_4(THF)_2](BF_4)$ in THF, followed by vapour diffusion of toluene under inert atmosphere, afforded the polymeric chain **2b** in good yield as tiny red-brown rods (see Equation (1) with L = THF, x = 1). Crystals of **2b** are air stable but only suitable for X-ray diffraction experiments using synchrotron radiation. The compound crystallizes in the monoclinic space group Pn with two tetrairon(III) SMMs, two diruthenium complexes and two BF_4^- anions in the asymmetric unit. The pyridyl nitrogen atoms of Fe_4 clusters coordinate the ruthenium atoms in the apical position replacing THF molecules, and generating two crystallographically-independent 1D chains that run along the **c** axis (Figures 2 and S2). Selected geometrical parameters, reported in Table S1, show that the two chains are structurally very similar, as are the Fe_4 units in **2b** and **1**·2EtOH. For example, the $Fe^c\cdots Fe^p$ distances are all in the 3.08–3.13 Å range. The pitch of the propeller-like Fe_4O_6 cores, evaluated as the average dihedral angle between the $Fe^c(O)_2Fe^p$ and Fe_4 planes is 68.7° in **1**·2EtOH and 70.1° in **2b**, hence typical of Fe_4 clusters with tripodal ligands.[14] The Fe^c–Ru separations are all very similar (av.: 9.6 Å) and the intrachain $Fe^c\cdots Fe^c$ distance, which equals the c unit cell axis length, is 21.3 Å. Neighbouring chains are closely packed, with BF_4^- anions occupying the cavities in between them (Figure S2); the shortest interchain $Fe^c\cdots Fe^c$ distance is 13.4 Å, while the minimum Fe···Fe separation is 9.9 Å. The two crystallographically-independent Fe_4 molecules are almost coplanar (5.4°) while the dihedral angle between Fe_4 and RuO_4 planes ranges from 23.8 to 25.3° (av.: = 24.5°).

Similarities between the structures of **2a** and **2b** emerged clearly from their IR absorption bands and Matrix-Assisted Laser Desorption/ Ionization-Time Of Flight (MALDI-TOF) mass spectra. In both compounds, the C=O and C=N stretching bands due to dpm^- and pPy^{3-} ligands (1500–1600 cm^{-1}) change their relative intensities as compared with **1** and signals due to acetato ligands appear at 1433 and 691 cm^{-1} in **2a** and at 1444 and 691 cm^{-1} in **2b**; the latter also shows a BF_4^- band at 1084 cm^{-1}, which is absent in **2a** (Figure S3). The positive-ion MALDI-TOF mass spectra of **2a** and **2b** display an isotopic cluster of the diad $[Fe_4(dpm)_6(pPy)_2][Ru_2(OAc)_4]^+$ centred at m/z 2122.5 (Figure S4 and Table S2).

The temperature dependence of the low field (1−10 kOe) molar magnetic susceptibility (χ_M) for **1**·2EtOH, **2a** and **2b** was measured between 1.9 and 300 K along with field-dependent isothermal molar magnetization (M_M) data at 4.5, 2.5 and 1.9 K. The $\chi_M T$-vs-T and M_M-vs-H/T curves, reported in Figure S5, are typical of Fe_4 systems,[14] with **2b** significantly more magnetic than the other two compounds, in accordance with the extra contribution of the s = 3/2 Ru_2 unit.[18] As Fe_4–Ru_2 magnetic interactions are expected to cover a much smaller energy scale than intramolecular Fe–Fe couplings and magnetic anisotropies, we assumed independent Fe_4 and Ru_2 units and simply subtracted the expected Ru_2 contribution from the data using typical g-values and zero-field splitting (zfs) parameters (D') for $Ru^{II,II}{}_2$ (s = 1, g_{Ru} = 2.15 and D' = 270 cm^{-1})[18,19] and $Ru^{II,III}{}_2$ (s = 3/2, g_{Ru} = 2.08 and D' = 63 cm^{-1}).[18,20] The resulting data were satisfactorily reproduced by Heisenberg (for $\chi_M T$-vs-T) or axial zfs (for M_M-vs-H) Hamiltonians with parameters typical for Fe_4 SMMs (see Supporting Information).[14]

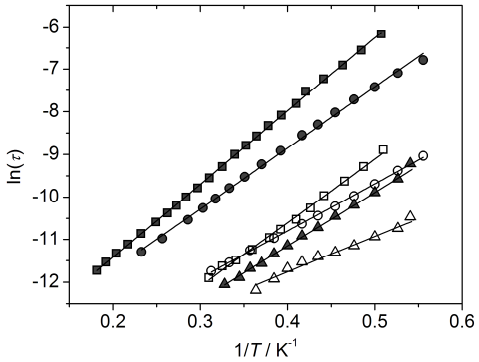

Figure 3. Arrhenius plots for compounds **1**·2EtOH (□), **2a** (○) and **2b** (△) obtained from ac susceptibility measurements in zero (empty symbols) and 1-kOe (filled symbols) applied static fields.

The magnetization dynamics of **1**·2EtOH, **2a** and **2b** was then investigated by alternating current (ac) susceptibility measurements at temperatures above 1.8 K and in both zero and 1-kOe applied static field. This *H* value was found most effective in minimizing quantum tunnelling (QT) effects. In all cases a temperature dependence of the maxima in the χ_M''-vs-*v* plots was observed (see Figure S6), demonstrating that the three compounds behave as SMMs. Within the Debye model[21] commonly employed to analyse ac response, a maximum in χ_M'' is observed when the relaxation time τ equals $(2\pi\nu)^{-1}$. The linear ln(τ)-vs-1/*T* dependence in the Arrhenius plots of Figure 3 indicates thermally activated relaxation mechanisms in the explored temperature range (see Table S3 for the best-fit parameters). Significantly, while the zfs *D* values remain similar in the three compounds, the anisotropy barriers U_{eff}/k_B follow the trend **2b** (12.63(7) K) < **2a** (14.30(17) K) < **1**·2EtOH (17.20(7) K) at 1 kOe, indicating that both $Ru^{II,II}_2$ and $Ru^{II,III}_2$ bridges enhance underbarrier relaxation over isolated Fe_4 units. The greater effect of $Ru^{II,III}_2$ is explained by the m = ±1/2 doublet stabilized by the large positive zfs, as opposed to the m = 0 singlet of $Ru^{II,II}_2$ (in the following, the Fe_4 and Ru_2 spin substates will be labelled by *M* and *m* quantum numbers). The two complexes then behave as effective s_{eff} = ½ and 0, respectively (Figure 1), and fast fluctuations of the former may provide a source of QT (see below). Zero-field ac measurements show shorter τ values and lower barriers but a similar trend in the three compounds. All measurements indicate a narrow distribution of relaxation times, with in-field α values[21] ranging from 0.13 to 0.17 at 1.9 K (see Supporting Information).

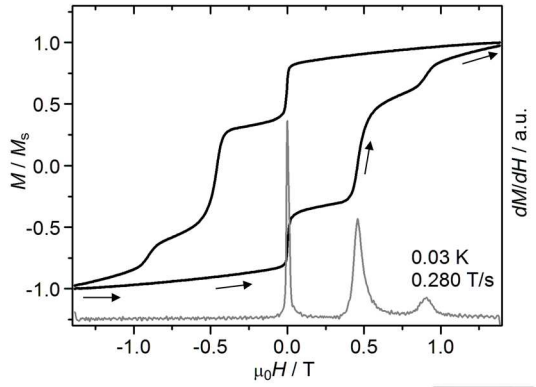

Figure 4. Magnetization versus dc field hysteresis loops for a single crystal of **2a** along with *dM*/*dH* curve (grey).

To probe the electronic structure over a much smaller energy scale, magnetic hysteresis loops were recorded on single crystals of **1**·2EtOH, **2a** and **2b** using a microSQUID apparatus and applying the magnetic field along the easy axis. In all cases, coercivity was found to increase with decreasing temperature and increasing scan rate, as expected for SMM behaviour, but the loops have a distinctly different shape in the three compounds. Measurements on **1**·2EtOH showed that QT-driven relaxation is reached below 0.3 K. Faster relaxation due to resonant QT of individual Fe_4 centres leads to steps in the hysteresis loops at regular field intervals of $|D|/(g\mu_B)$ ~ 0.5 T (see Figures S7 and S8), with pre-step features typical of spin-spin cross relaxation promoted by intermolecular dipole-dipole interactions.[22] Dipolar interactions through the lattice also shift the "zero-field" QT resonance slightly to positive fields (ca. 10 mT), in accordance with previous findings;[22] such relaxation process around zero field remains visible even at the lowest temperature (0.03 K) and with the fastest scan rate (0.28 T/s).

The hysteresis loops of **2a** (Figures 4, S9 and S10) closely resemble those of **1**·2EtOH. Magnetization steps are detected at 0.00, 0.46 and 0.90 T, in agreement with the behaviour of isolated Fe_4 units. The absence of intrachain communication is again explained by considering the integer spin and huge positive zfs of the $Ru^{II,II}_2$ complex, which result in a nonmagnetic m = 0 ground state (Figure 1).

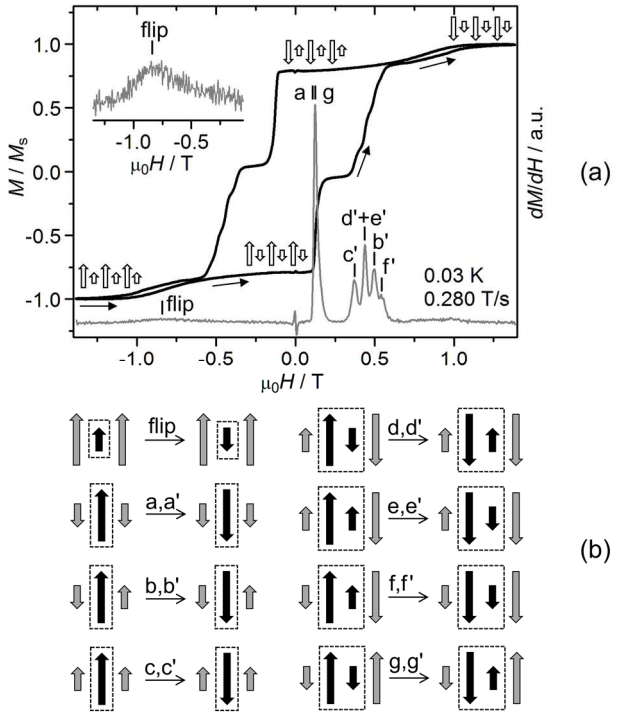

Figure 5. (a) Magnetization versus dc field hysteresis loop for a single crystal of **2b**, along with the *dM*/*dH* curve (grey). Vertical ticks mark the spin-flip transition and the QT resonances. The derivative signal at H = 0 is an instrumental artifact. M_s is saturation magnetization. (b) Proposed assignment of the steps in the hysteresis loop, with spins rotated by 90° from the chain direction for a simpler representation. Spins undergoing reversal are drawn as black arrows and highlighted by a dashed rectangle, while spins remaining fixed are in grey. Unprimed and primed letters denote M = +5 → –5 and M = +5 → –4, resonances, respectively.

The behaviour of **2b** is remarkably different (Figures 5a, S11 and S12). At 0.03 K coercivity is reduced as compared with **1**·2EtOH but a large remnant magnetization, amounting to ca. 79% of saturation magnetization (M_s), is found in zero field at all sweep rates explored. Saturation is reached in applied fields larger than ca. 1 T following a broad, quasireversible step at ±0.84(1) T. Such enhanced memory effect originates from a pronounced shift of the "zero-field" resonance to ±0.124 T. A second, pronounced magnetization step is detected between 0.37 and 0.54 T (Figure 5a), *i.e.* close to the field ($|D|/(g\mu_B)$) where the M = +5 to –4 transition typically occurs in isolated Fe_4

complexes.[22] Since dipolar fields within a chain and between chains would not exceed a few mT in both compounds, the observed differences in magnetic behaviour must arise from superexchange interactions with the Ru_2 units rather than from crystal packing effects.

Assuming that no interchain interactions are operative (see above), the behaviour of **2b** can be described by a chain model of alternating anisotropic $S = 5$ and $s = 3/2$ spins weakly coupled via Heisenberg exchange. However, as detailed in Supporting Information, the low-lying spin levels are accurately reproduced by an Ising-like model where only spin components along the Fe_4 easy axis are relevant:

$$E = D \Sigma_i M_{2i}^2 + \Sigma_i J_{|M|} M_{2i}(m_{2i-1}+m_{2i+1}) + \mu_B B \Sigma_i (g M_{2i} + g_{eff} m_{2i-1}) \quad (2)$$

The first term accounts for magnetic anisotropy at Fe_4 centres that are located on even-i sites. The Ru_2 complexes occupy odd-i sites and, owing to their large hard-axis anisotropy, are described by $m = \pm 1/2$ and an anisotropic g-factor $g_{eff} = (g_{II}^2 \cos^2\theta + g_{\perp}^2 \sin^2\theta)^{1/2}$, with $g_{II} = g_{Ru}$ and $g_{\perp} = 2g_{Ru}$.[23] Here, θ is the angle between the Fe_4 and Ru_2 anisotropy axes ($\theta \sim 25°$ from crystal structure, whence $g_{eff} \sim 2.60$) $J_{|M|}$ is the effective Fe_4–Ru_2 exchange-coupling constant, which can be different depending on whether the Fe_4 complex occupies the $M = \pm 5$ or the $M = \pm 4$ doublet (see Supporting Information). Differences with the electronic structure of **2a** are pictured in Figure 1.

We now analyse the field dependence of the magnetization in terms of the most probable tunneling events, i.e. individual or pairwise spin reversals, following the pathway marked by arrows in Figure 5a. The application of a large negative ("down") field aligns all the spins in the upward direction, *i.e.* $M = +5$ and $m = +1/2$ at all sites. As the field magnitude declines, the broad step detected at –0.84(1) T is suggestive of *antiferromagnetic* Fe_4–Ru_2 coupling and of a spin flip transition, whereby all Ru_2 spins reverse to $m = -1/2$. At the transition field, the decrease in exchange energy exactly equals the increase in Zeeman energy, *i.e.* $B_{flip} = 10J_5/(g_{eff}\mu_B)$, whence $J_5 \sim 0.10$ cm^{-1} for $g_{eff} \sim 2.60$. By consequence an effective *ferromagnetic* coupling is established between Fe_4 units, a rare situation in supramolecular SMM assemblies.[9f,24] This coupling strength confirms that in the temperature range explored by ac susceptibility measurements the condition $k_BT > 10J_5$ holds and substantial fluctuations of $Ru^{II,III}_2$ spins are to be expected. After the spin-flip transition, the magnetization remains virtually constant up to ca. 0.10 T and no zero-field QT resonance is detected. In fact, for a resonant tunnelling event to occur the initial and final states must have the same energy, *i.e.* the decrease in Zeeman energy upon QT must exactly compensate the increase in exchange and anisotropy energies. It is straightforward to show that, for a given Fe_4 centre in the chain, the QT transitions from $M = +5$ to –5 and from $M = +5$ to –4 are split into three depending on the $m_{L(R)}$ value of its lefthand L (righthand R) Ru_2 neighbours, in much the same way as a ^{1}H nucleus coupled to two equivalent neighbouring protons gives a triplet in NMR spectra. The two groups of resonances, labelled a,b,c and a',b',c' in Figure 5b, should occur at fields

$$B = -J_5(m_L+m_R)/(g\mu_B) \quad (3a)$$

$$B' = |D|/(g\mu_B) - [(5/9)J_5+(4/9)J_4](m_L+m_R)/(g\mu_B) \quad (3b)$$

Then, the term proportional to m_L+m_R may be conveniently viewed as "bias field" that adds to the external field B and shifts the resonances. Because after the spin flip transition all Fe_4 spins are "up" ($M = +5$) and all Ru_2 spins are "down" ($m = -1/2$), relaxation around zero field may only start through a QT resonance involving this initial state (resonance a in our scheme). Setting $J_5 = 0.10$ cm^{-1} and $m_L = m_R = -1/2$ in Equation (3a) one finds $B = 0.11$ T, in reasonable agreement with the sharp increase of the magnetization at 0.124 T. The further increase of the magnetization between 0.37 and 0.54 T occurs in four substeps at 0.374, 0.439, 0.494 and 0.545 T, as most clearly shown by the first-derivative curve in Figure 5a. The spacing between the first and third substeps (0.120 T) is virtually identical to the bias field that affects the "zero field" resonance, suggesting that exchange energy may be at the origin of the observed fine structure. When the first and third substeps are assigned to resonances c' and b' (*i.e.* $m_L+m_R = 1$ and 0 in Eq. 3b), it follows that $D = -0.46$ cm^{-1}, a realistic value for Fe_4 complexes. With this assignment, resonance a' would occur at 0.61 T, i.e. in a field region where "up" Fe_4 spins are no longer available. It is important to notice here that approximately half of the Fe_4 spins have already reversed at around 0.2-0.3 T, so that $m_L = m_R = -1/2$ is by no means the only accessible initial state. The two remaining substeps are not accounted for by the exchange-biased flipping of individual Fe_4 spins, but can be explained by the simultaneous reversal of a Fe_4 spin *and* a neighbouring Ru_2 unit. Considering the spin arrangement within the pair and the orientation of the two adjacent spins, eight different QT events of this type can be envisaged, whose resonant fields are easily worked out from Equation (2) (see Supporting Information). Among them, three resonances are indeed predicted at 0.452 (d'), 0.431 (e') and 0.525 T (f'), hence close to the second and fourth substeps (see Figure 5b). In addition, resonance g is expected at 0.123 T and can also contribute to the relaxation step around zero field, for it has the same initial state as resonance a. With this assignment, all step positions are reproduced within 4 mT using the following set of spin Hamiltonian parameters: $g = 2.00$ (fixed), $D = -0.465(2)$ cm^{-1}, $J_5 = 0.101(1)$ cm^{-1}, $J_4 = 0.133(7)$ cm^{-1} and $g_{eff} = 2.57(4)$. Notice that the best-fit g_{eff} value is fully consistent with the typical Landè factor of diruthenium(II,III) paddlewheels[18,20] and with the θ value estimated from the crystal structure. Moreover, the relative magnetization change at the spin flip transition $(5g-g_{eff}/2)/(5g+g_{eff}/2) = 0.77$ is in good agreement with the measured value (0.79). All experimental features are thus reproduced with great accuracy by our relatively simple model, confirming that Fe_4 clusters are an ideal work bench for investigating quantum effects in the dynamics of the magnetization.

In conclusion, we have harnessed the chemical versatility of Fe_4 complexes to prepare chain-like assemblies of SMM units bridged by diruthenium paddlewheels in two different oxidation states. The diruthenium(II,II) bridges in **2a** have $s = 1$, but their huge hard-axis anisotropy results in a nonmagnetic $m = 0$ ground singlet and in negligible intrachain communication. By contrast, the diruthenium(II,III) bridges have half-integer ($s = 3/2$) spin while maintaining a large hard-axis anisotropy. By virtue of their $m = \pm 1/2$ ground doublet, they act as effective magnetic couplers and compound **2b** behaves as a significantly better

magnet in zero-field than an array of non-interacting Fe_4 centres. This new behaviour suggests the possibility to prepare redox-responsive SMMs arrays in which intrachain coupling and remnant magnetization are reversibly tuned by electron transfer.

Experimental Section

General procedures. All operations for the syntheses of compounds **2a** and **2b** were carried out with strict exclusion of moisture into a drybox. For the synthesis of compound **1**·2EtOH and other general synthetic details, X-ray crystal structure determinations and magnetic measurements see the Supporting Information.

2a: A light brown solution of $[Ru_2(OAc)_4(MeOH)_2]$ (50 mg, 0.099 mmol) in anhydrous THF (20 mL) was layered over a red solution of compound **1**·2EtOH (168 mg, 0.0946 mmol) in anhydrous DCM (20 mL) with a 2-mL layer of clean DCM in between, and left to liquid diffusion for ten days. Tiny red crystals of the title compound formed, that can be isolated, washed with *n*-hexane and dried (129 mg, 64.2%). In order to preserve the crystallinity, the compound has to be kept in its mother liquor or into grease. Elemental analysis calcd for $C_{92}H_{146}Fe_4N_2O_{26}Ru_2$ (2121.66): C, 52.08; H, 6.94; N, 1.32. Found for dried sample: C, 51.79; H, 7.05; N, 1.40. IR (KBr): 2960 ν(C–H_{tBu}), 1592, 1576, 1564, 1549, 1505 ν(C=O_{dpm}, C=N_{py}), 1433 ν(C=O_{AcO}), 1401, 1385, 1357 ν(CH_3), 1106 ν(C–O_{pPy}), 689 δ(AcO), 565 δ(py) cm^{-1}. MALDI-TOF (THF): *m/z* 2122.52 ($[M]^+$, 5%), 1721.58 ($[Fe_4(pPy)_2(dpm)_6 + K]^+$, 2), 1705.61 ($[Fe_4(pPy)_2(dpm)_6 + Na]^+$, 2), 1499.49 ($[Fe_4(pPy)_2(dpm)_5)]^+$, 30), 1316.34 ($[Fe_4(pPy)_2(dpm)_4)]^+$, 90), 439.79 ($[Ru_2(OAc)_4]^+$, 40), 422.16 ($[Fe(dpm)_2]^+$, 100).

2b: Compound **1**·2EtOH (101 mg, 0.0569 mmol) and $[Ru_2(OAc)_4(THF)_2](BF_4)$ (40 mg, 0.060 mmol) were dissolved in anhydrous THF (20 and 12 mL, respectively) and mixed together. Slow vapor diffusion of anhydrous toluene (42 mL) gave the title compound as tiny red/brown crystals, which were extensively washed with anhydrous dichloromethane till colorless washings (97.5 mg, 77.6%). Elemental analysis calcd for $C_{92}H_{146}BF_4Fe_4N_2O_{26}Ru_2$ (2208.47): C, 50.03; H, 6.66; N, 1.27. Found: C, 49.69; H, 6.92; N, 1.41. IR (KBr): 2964 ν(C–H_{tBu}), 1592, 1576, 1564, 1549, 1538, 1505 ν(C=O_{dpm}, C=N_{py}), 1444 ν(C=O_{AcO}), 1401, 1385, 1357 ν(CH_3), 1107 ν(C–O_{pPy}), 1084 ν(BF_4), 691 δ(AcO), 564 δ(py) cm^{-1}. MALDI-TOF (THF): *m/z* 2122.41 ($[M – BF_4]^+$, 5%), 1499.41 ($[Fe_4(pPy)_2(dpm)_5)]^+$, 20), 1316.28 ($[Fe_4(pPy)_2(dpm)_4)]^+$, 30), 438.81 ($[Ru_2(OAc)_4]^+$, 40), 422.15 ($[Fe(dpm)_2]^+$, 100).

Acknowledgements

Authors would like to thank the European Research Council and the Italian MIUR for funding through the Advanced Grant MolNanoMas (no. 267746) and a FIRB project (RBAP117RWN), respectively, and Dr. Giordano Poneti (University of Firenze) for his help with the magnetic measurements.

Keywords: 1D coordination polymers, Exchange bias, Fe_4 clusters, Ruthenium dimers, Single-molecule magnets

[1] D. Gatteschi, R. Sessoli, J. Villain, *Molecular Nanomagnets*, Oxford University Press, Oxford, **2006**.

[2] a) S. Thiele, F. Balestro, R. Ballou, S. Klyatskaya, M. Ruben and W. Wernsdorfer, *Science* **2014**, *344*, 1135–1138; b) R. Vincent, S. Klyatskaya, M. Ruben, W. Wernsdorfer, F. Balestro, *Nature* **2012**, *488*, 357–360.

[3] M. N. Leuenberger, D. Loss, *Nature* **2001**, *410*, 789–793.

[4] a) F. Troiani, M. Affronte, *Chem. Soc. Rev.* **2011**, *40*, 3119–3129; b) C. J. Wedge, G. A. Timco, E. T. Spielberg, R. E. George, F. Tuna, S. Rigby, E. J. L. McInnes, R. E. P. Winpenny, S. J. Blundell, A. Ardavan, *Phys. Rev. Lett.* **2012**, *108*, 107204.

[5] A. Cornia, M. Mannini, *Struct. Bond.* **2014**, DOI: 10.1007/430_2014_150.

[6] a) W. Wernsdorfer, N. Aliaga-Alcalde, D. N. Hendrickson, G. Christou, *Nature* **2002**, *416*, 406–409; b) S. Hill, R. S. Edwards, N. Aliaga-Alcalde, G. Christou, *Science* **2003**, *302*, 1015–1018; c) R. Tiron, W. Wernsdorfer, D. Foguet-Albiol, N. Aliaga-Alcalde, G. Christou, *Phys. Rev. Lett.* **2003**, *91*, 227203.

[7] R. Bagai, W. Wernsdorfer, K. A. Abboud, G. Christou, *J. Am. Chem. Soc.* **2007**, *129*, 12918–12919.

[8] L. Lecren, W. Wernsdorfer, W.-G. Li, A. Vindigni, H. Miyasaka, R. Clérac, *J. Am. Chem. Soc*. **2007**, *129*, 5045–5051.

[9] a) R. Tiron, W. Wernsdorfer, N. Aliaga-Alcalde, G. Christou, *Phys. Rev. B.* **2003**, *68*, 140407; b) E.-C. Yang, W. Wernsdorfer, S. Hill, R. S. Edwards, M. Nakano, S. Maccagnano, L. N. Zakharov, A. L. Rheingold, G. Christou, D. N. Hendrickson, *Polyhedron* **2003**, *22*, 1727–1733; c) E.-C. Yang, W. Wernsdorfer, L. N. Zakharov, Y. Karaki, A. Yamaguchi, R. M. Isidro, G.-D. Lu, S. A. Wilson, A. L. Rheingold, H. Ishimoto, D. N. Hedrickson, *Inorg. Chem.* **2006**, *45*, 529–546; d) R. Inglis, L. F. Jones, K. Mason, A. Collins, S. A. Moggach, S. Parsons, S. P. Perlepes, W. Wernsdorfer, E. K. Brechin, *Chem. Eur. J.* **2008**, *14*, 9117–9121; e) R. Inglis, S. M. Taylor, L. F. Jones, G. S. Papaefstathiou, S. P. Perlepes, S. Datta, S. Hill, W. Wernsdorfer, E. K. Brechin, *Dalton Trans.* **2009**, 9157–9168; f) A. Das, K. Gieb, Y. Krupskaya, S. Demeshko, S. Dechert, R. Klingeler, V. Kataev, B. Buchner, P. Muller, F. J. Meyer, *J. Am. Chem. Soc.* **2011**, *133*, 3433–3443.

[10] T. N. Nguyen, W. Wernsdorfer, K. A. Abboud, G. Christou, *J. Am. Chem. Soc.* **2011**, *133*, 20688–20691.

[11] J. Yoo, W. Wernsdorfer, E.-C. Yang, M. Nakano, A. L. Rheingold, D. N. Hendrickson, *Inorg. Chem.* **2005**, *44*, 3377–3379.

[12] a) L. Lecren, O. Roubeau, Y.-G. Li, X. F. Le Goff, H. Miyasaka, F. Richard, W. Wernsdorfer, C. Coulon, R. Clérac, *Dalton Trans.* **2008**, 755–766; b) L. Lecren, O. Roubeau, C. Coulon, Y.-G. Li, X. F. Le Goff, W. Wernsdorfer, H. Miyasaka, R. Clérac, *J. Am. Chem. Soc.* **2005**, *127*, 17353–17363.

[13] a) K. S. Pedersen, J. Bendix, R. Clérac, *Chem. Commun.* **2014**, *50*, 4396–4415; b) I.-E. Jeon, R. Clérac, *Dalton Trans.* **2012**, *41*, 9569–9586.

[14] a) S. Accorsi, A.-L. Barra, A. Caneschi, G. Chastanet, A. Cornia, A. C. Fabretti, D. Gatteschi, C. Mortalò, E. Olivieri, F. Parenti, P. Rosa, R. Sessoli, L. Sorace, W. Wernsdorfer, L. Zobbi, *J. Am. Chem. Soc*. **2006**, *128*, 4742–4755; b) L. Gregoli, C. Danieli, A.-L. Barra, P. Neugebauer, G. Pellegrino, G. Poneti, R. Sessoli, A. Cornia, *Chem. Eur. J.* **2009**, *15*, 6456–6467; c) M. J. Rodriguez-Douton, A. Cornia, R. Sessoli, L. Sorace, A.-L. Barra, *Dalton Trans.* **2010**, *39*, 5851−5859; d) T. K. Prasad, G. Poneti, L. Sorace, M. J. Rodriguez-Douton, A.-L. Barra, P. Neugebauer, L. Costantino, R. Sessoli, A. Cornia, *Dalton Trans.* **2012**, *41*, 8368−8378.

[15] M. C. Barral, R. González-Prieto, R. Jiménez-Aparicio, J. L. Priego, M. R. Torres, F. A. Urbanos, *Inorg. Chim. Acta* **2005**, *358*, 217–221.

[16] F. A. Urbanos, M. C. Barral, R. Jimenez-Aparicio, *Polyhedron* **1998**, *7*, 24, 2597–2600.

[17] a) M. Affronte, I. Casson, M. Evangelisti, A. Candini, S. Carretta, C. A. Muryn, S. J. Teat, G. A. Timco, W. Wernsdorfer, R. E. P. Winpenny, *Angew. Chem. Int. Ed.* **2005**, *44*, 6496–6500; b) M. Affronte, F. Troiani, A. Ghirri, S. Carretta, P. Santini, V. Corradini, R. Schuecker, C. Muryn, G. Timco, R. E. Winpenny, *Dalton Trans*. **2006**, 2810–2817; c) G. A. Timco, S. Carretta, F. Troiani, F. Tuna, R. J. Pritchard, C. A. Muryn, E. J. L. McInnes, A. Ghirri, A. Candini, P. Santini, G. Amoretti, M. Affronte, R. E. P. Winpenny, *Nat. Nanotechnol.* **2009**, *4*, 173–178; d) G. F. S. Whitehead, B. Cross, L. Carthy, V. A. Milway, H. Rath, A. Fernandez, S. L. Heath, C. A. Muryn, R. G. Pritchard, S. J. Teat, G. A. Timco, R. E.

P. Winpenny, *Chem. Commun.* **2013**, *49*, 7195–7197; e) M. Affronte, F. Troiani, A. Ghirri, S. Carretta, P. Santini, R. Schuecker, G. Timco, R. E. P. Winpenny, *J. Magn. Magn. Mater.* **2007**, *310*, e501–e502.

[18] a) M. A. S. Aquino, *Coord. Chem. Rev.* **1998**, *170*, 141–202; b) M. Mikuriya, D. Yoshioka, M. Handa, *Coord. Chem. Rev.* **2006**, *250*, 2194–2211.

[19] M. Handa, D. Yoshioka, M. Mikuriya, I. Hiromitsu, K. Kasuga, *Mol. Cryst. Liq. Cryst.* **2002**, *376*, 257–262.

[20] a) F. D. Cukiernik, A.-M. Giroud-Godquin, P. Maldivi, J.-C. Marchon, *Inorg. Chim. Acta* **1994**, *215*, 203–207; b) E. J. Beck, K. D. Drysdale, L.K. Thompson, L. Li, C. A. Murphy, M. A. S. Aquino, *Inorg. Chim. Acta* **1998,** *279*, 121–125.

[21] a) K. S. Cole, R. H. Cole, *J. Chem. Phys.* **1941**, *9*, 341−352; b) C. Dekker, A. F. M. Arts, H. W. Wijn, A. J. Van Duyneveldt, J. A. Mydosh, *Phys Rev. B* **1989**, *40*, 11243−11251.

[22] L. Vergnani, A.-L. Barra, P. Neugebauer, M. J. Rodriguez-Douton, R. Sessoli , L. Sorace, W. Wernsdorfer, A. Cornia, *Chem. Eur. J.* **2012**, *18*, 3390–3398.

[23] R. D. L. Carlin, *Magnetochemistry*, Springer, Berlin, **1986**.

[24] W. Wernsdorfer, S. Bhaduri, A. Vinslava, G. Christou, *Phys. Rev. B* **2005**, *72*, 214429.